Oxygen Vacancies

International Edition: DOI: 10.1002/anie.201600687
German Edition: DOI: 10.1002/ange.201600687

Plasma-Engraved Co_3O_4 Nanosheets with Oxygen Vacancies and High Surface Area for the Oxygen Evolution Reaction

Lei Xu, Qianqian Jiang, Zhaohui Xiao, Xingyue Li, Jia Huo, Shuangyin Wang, and Liming Dai*

Abstract: *Co_3O_4, which is of mixed valences Co^{2+} and Co^{3+}, has been extensively investigated as an efficient electrocatalyst for the oxygen evolution reaction (OER). The proper control of Co^{2+}/Co^{3+} ratio in Co_3O_4 could lead to modifications on its electronic and thus catalytic properties. Herein, we designed an efficient Co_3O_4-based OER electrocatalyst by a plasma-engraving strategy, which not only produced higher surface area, but also generated oxygen vacancies on Co_3O_4 surface with more Co^{2+} formed. The increased surface area ensures the Co_3O_4 has more sites for OER, and generated oxygen vacancies on Co_3O_4 surface improve the electronic conductivity and create more active defects for OER. Compared to pristine Co_3O_4, the engraved Co_3O_4 exhibits a much higher current density and a lower onset potential. The specific activity of the plasma-engraved Co_3O_4 nanosheets ($0.055\ mA\,cm^{-2}_{BET}$ at 1.6 V) is 10 times higher than that of pristine Co_3O_4, which is contributed by the surface oxygen vacancies.*

Electrocatalytic water splitting provides a sustainable strategy to supply clean energy through hydrogen evolution reaction (HER) and oxygen evolution reaction (OER), where an effective catalyst is a necessity.[1] In principle, OER is a thermodynamic uphill reaction involving a stepwise four-electron transfer at a high overpotential. Noble metal/metal oxides, such as Pt, RuO_2, and IrO_2, are still considered as being the most active electrocatalysts. However, the high cost and element scarcity of these noble metals or metal oxides seriously hinder their large-scale application for water splitting. Co-based oxides can act as active OER electrocatalysts with relatively low cost and earth-abundance. Bulk cobalt oxides are normally less active for OER due to their poor conductivity and low surface area. The electrocatalytic activity of cobalt oxide is mainly determined by its surface area and electronic states. Various approaches have been adopted to improve the catalytic activity of cobalt oxides for OER.[2] Anchoring Co_3O_4 nanocrystals on carbon-based supports could significantly enhance their electrocatalytic activity for OER contributed by the small crystalline size and conductive support.[3]

As discussed above, the electrocatalytic activity of Co_3O_4 was mainly affected by its surface area and electronic states. The higher surface area of Co_3O_4 provides more accessible sites for electrochemical reactions. The surface area could be increased through a nanostructure strategy.[4] On the other hand, the electronic states, especially the surface electronic states, of Co_3O_4 could be tuned by doping with a third element,[5] facet control,[6] or oxygen vacancies.[7] Tuning oxygen vacancies of metal oxides could significantly alter their catalytic activity.[8] Co_3O_4 is of mixed valences with the presence of Co^{2+} and Co^{3+}. The proper control of the ratio of Co^{2+}/Co^{3+} in the Co_3O_4 could lead to significant modifications on its electronic and thus catalytic properties.[7]

Herein, we designed a highly efficient Co_3O_4-based OER electrocatalyst with oxygen vacancies and high surface area by a one-step plasma-engraving strategy. The pristine Co_3O_4 nanosheets were deposited on a Ti substrate by the electrodeposition of $Co(OH)_2$ followed by thermal annealing. The pristine Co_3O_4 nanosheets were subjected to the Ar plasma treatment. It is well known that the Ar plasma is often used for etching and cleaning.[9] The Ar plasma treatment on Co_3O_4 nanosheets could effectively engrave the nanosheet structure to expose more surface sites, as illustrated in Scheme 1. More

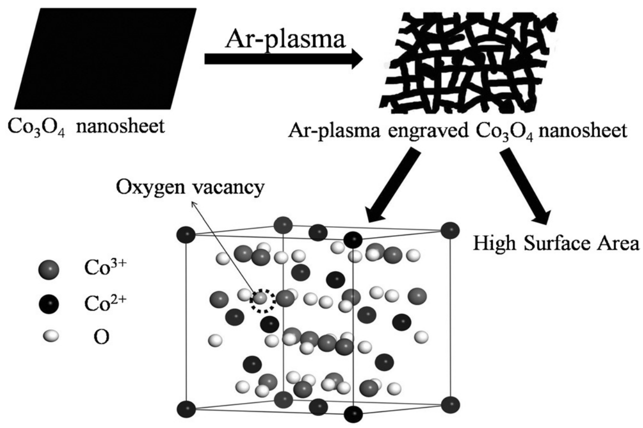

Scheme 1. Illustration of the preparation of the Ar-plasma-engraved Co_3O_4 with oxygen vacancies and high surface area.

surprisingly, the plasma-engraved Co_3O_4 shows the presence of oxygen vacancies on its surface, as characterized by XRD and XPS. The increased surface area and the generated surface oxygen vacancies of Co_3O_4 by the plasma engraving significantly contributed to the excellent electrocatalytic performance for OER. Compared to the pristine Co_3O_4 nanosheets, the plasma-engraved Co_3O_4 nanosheets exhibit

[*] L. Xu, Q. Jiang, Z. Xiao, X. Li, J. Huo, Prof. S. Wang
State Key Laboratory of Chem/Bio-Sensing and Chemometrics
College of Chemistry and Chemical Engineering
Hunan University, Changsha, 410082 (P.R. China)
E-mail: shuangyinwang@hnu.edu.cn
Prof. L. Dai
Department of Macromolecule Science and Engineering
Case Western Reserve University, Ohio (USA)

Supporting information for this article can be found under: http://dx.doi.org/10.1002/anie.201600687.

a much higher current density of 44.44 $mA\,cm^{-2}$ at 1.6 V vs. reversible hydrogen electrode (RHE) and a much lower onset potential of 1.45 V. The specific activity of plasma-engraved Co_3O_4 nanosheets obtained by normalizing the OER current with the BET surface area (0.055 $mA\,cm^{-2}{}_{BET}$ at 1.6 V) is 10 times higher than that of pristine Co_3O_4 nanosheets. It should be pointed out that the Ar plasma treatment is very time-saving with only 120 s to produce highly efficient electrocatalyts, and the similar strategy could be extended to engrave NiO nanosheets with improved electrocatalytic performance for OER as well.

For the preparation of Co_3O_4 nanosheets, $Co(OH)_2$ was electrochemically deposited on Ti foil followed by the thermal annealing to form Co_3O_4 nanosheets, which were treated by Ar plasma for 120 s. To observe the effect of the plasma treatment on the surface morphology of Co_3O_4 nanosheets, the SEM characterizations were performed. Figure 1 shows the SEM images of pristine and the plasma-

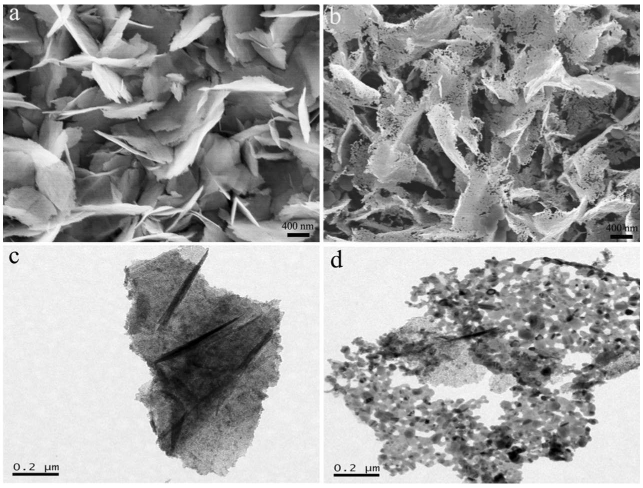

Figure 1. SEM images of a) pristine Co_3O_4 and b) Ar-plasma engraved Co_3O_4. TEM images of c) pristine Co_3O_4 and d) Ar-plasma engraved Co_3O_4.

engraved Co_3O_4 nanosheets. As shown, a continuous and compact surface was observed for pristine Co_3O_4 nanosheets. For the plasma-engraved Co_3O_4, the rough, discontinuous and loose surface was observed, in which the interconnected Co_3O_4 nanoparticles were observed. The SEM comparison clearly demonstrated that the plasma treatment could effectively engrave Co_3O_4 nanosheets to increase the surface area. We also engraved Co_3O_4 nanosheets for different times (Supporting Information, Figure S1). It could be found that more Co_3O_4 species were etched off with the increase of the plasma-engraving time. To further investigate the structural change of Co_3O_4 nanosheets after the plasma treatment, TEM characterizations were performed on both pristine Co_3O_4 and plasma-engraved Co_3O_4, as shown in Figure 2. Like the SEM observation, solid and compact nanosheets were observed on pristine Co_3O_4. For plasma-engraved Co_3O_4, the interconnected Co_3O_4 nanostructures with amounts of nanoholes were observed. Obviously, it can be seen that the plasma-engraved Co_3O_4 have a much higher surface area per unit mass,

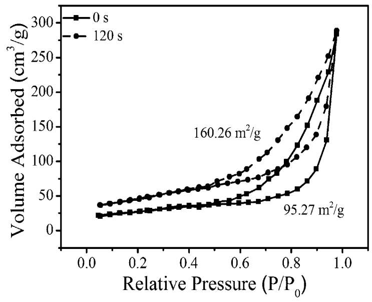

Figure 2. N_2 sorption isotherms of pristine and plasma-engraved Co_3O_4.

resulting in enhanced electrochemical performance, as discussed below. To investigate the possible extension of the plasma-engraving strategy, we also treated NiO nanosheets by Ar plasma (Supporting Information, Figure S2), from which it could apparently be seen that the plasma could also effectively engrave NiO nanosheets with more exposed surface area per unit mass. This phenomenon could be more clearly observed in TEM images (Supporting Information, Figure S3).

The high-resolution TEM (HRTEM) is used to study the crystalline structure of Co_3O_4 nanosheets before and after the plasma engraving. From the HRTEM images (Supporting Information, Figure S4), the lattice spacing (220) of pristine Co_3O_4 nanosheets is 0.29 nm (Figure S4a,c), which is the same with the plasma-engraved Co_3O_4 nanosheet (Figure S4b,d). The lattice spacing of NiO nanosheet is the same (0.21 nm) before and after the plasma treatment (Supporting Information, Figure S5). XRD characterizations were also performed on both Co_3O_4 and NiO to observe the crystalline change before and after the plasma treatment. The XRD patterns (Supporting Information, Figure S6) of pristine Co_3O_4 and NiO nanosheets can be indexed to those in the JCPDS data (JCPDS No. 43-1003) and (JCPDS No. 44-1159), respectively. After the plasma treatment, the XRD patterns show no obvious change. Both HRTEM and XRD results indicated that the bulk crystalline phases of Co_3O_4 nanosheets were not significantly changed by the plasma engraving, although a higher surface area was obtained.

As observed by the SEM and TEM, it is believed that the plasma-engraved Co_3O_4 nanosheets would expose more surface area. To confirm this hypothesis, the N_2 sorption isotherms (Figure 2) were obtained for the two samples. The Brunauer–Emmett–Teller (BET) surface area of plasma-engraved Co_3O_4 is much higher than that of pristine Co_3O_4 (160.26 vs. 95.27 $m^2\,g^{-1}$). This comparison confirms that the plasma engraving could significantly increase the surface area of Co_3O_4, resulting in more exposed sites for the electrocatalysis, as discussed below.

Since the electrocatalysis reaction mainly occurs on the surface of electrocatalysts, it is essential to investigate the surface properties of Co_3O_4 before and after the plasma treatment.[10] The X-ray photoelectron spectroscopy is an ultra-sensitive tool to detect the surface properties of electrocatalysts.[11] XPS characterizations were performed on the pristine and the plasma-engraved Co_3O_4. The survey spectra (Supporting Information, Figure S7) show the presence of Co and O in both the samples. The fine-scanned Co 2p XPS spectra of the pristine and the plasma-engraved Co_3O_4 were given in Figure 3 a, in which the peaks of Co $2p_{3/2}$ and Co $2p_{1/2}$ located at around 780 eV and 796 eV, respectively, for both samples. Compared to the pristine Co_3O_4, the Co 2p peaks of the plasma-engraved Co_3O_4 exhibit two new satellite peaks centered at about 786 eV and about 803 eV (Figure 3 a), which is attributed to the Co^{2+} oxidation state, indicating that a portion of Co^{3+} ions is reduced to Co^{2+} with generating oxygen vacancies.[7] To get further insight into the surface properties, the fine-scanned Co 2p spectra of both pristine and plasma-engraved Co_3O_4 were fitted to investigate the electronic states of Co atoms with different valences (Figure 3 b,c). The two fitted peaks for Co $2p_{3/2}$ are Co^{3+} (ca. 779.5 eV) and Co^{2+} (ca. 780.8 eV), respectively.[12] The relative atomic ratio of Co^{2+}/Co^{3+} on the surface of the Co_3O_4 could be obtained by comparing the area that the fitted curve covered. It could be clearly observed that the atomic ratio of Co^{2+}/Co^{3+} (1.2) on the plasma-engraved Co_3O_4 is higher than that (1.0) of pristine Co_3O_4,indicating that relatively more Co^{2+} present in the plasma-engraved Co_3O_4, that is, surface oxygen vacancies were generated by Ar plasma, which can be confirmed by the fine-scanned O 1s XPS spectra. Figure 3 d shows two oxygen peaks contributions of O 1s region of pristine Co_3O_4 and Figure 3 e shows four oxygen peaks contributions of O 1s region of the engraved Co_3O_4. O1 at 529.8 eV is typical for metal–oxygen bonds, whereas O4 at the higher value of 532 eV resulted from Co_3O_4 reduction by Ar plasma attributed to the high-binding energy peak from surface oxygen defect species.[3,8,13] The appearance of the O4 peak in the O 1s region of the plasma-engraved Co_3O_4 indicates the presence of oxygen vacancies on the surface of Co_3O_4.[14] The fine-scanned XPS results of Co 2p region and O 1s region of pristine and plasma-engraved Co_3O_4 nanosheets indicated that Co^{3+} is partially reduced to Co^{2+}, producing oxygen vacancies. The partial reduction from Co^{3+} to Co^{2+} resulted from the Ar plasma treatment. Previously, Ar plasma has been used to reduce metal ions to metal nanoparticles, indicating its reducing capability.[15] Since XRD and HRTEM characterizations show no obvious change of the bulk phase of Co_3O_4 after the plasma treatment while XPS spectra indicates the appearance of oxygen vacancies, it is believed that the oxygen vacancies are only present on the surface of Co_3O_4. It is understandable as the plasma is a surface treatment technology.[16] Previous density-functional theory (DFT) calculations revealed that the oxygen vacancies create new defect states located in the band gap of Co_3O_4 and the two electrons on the defect states are easily excited, resulting in improvement of the conductivity of Co_3O_4.[7] The oxygen vacancies on the surface of Co_3O_4 formed by the plasma-engraving may improve the electronic conductivity, create more electrochemically active sites, and thus enhance the electrocatalytic activity for OER.

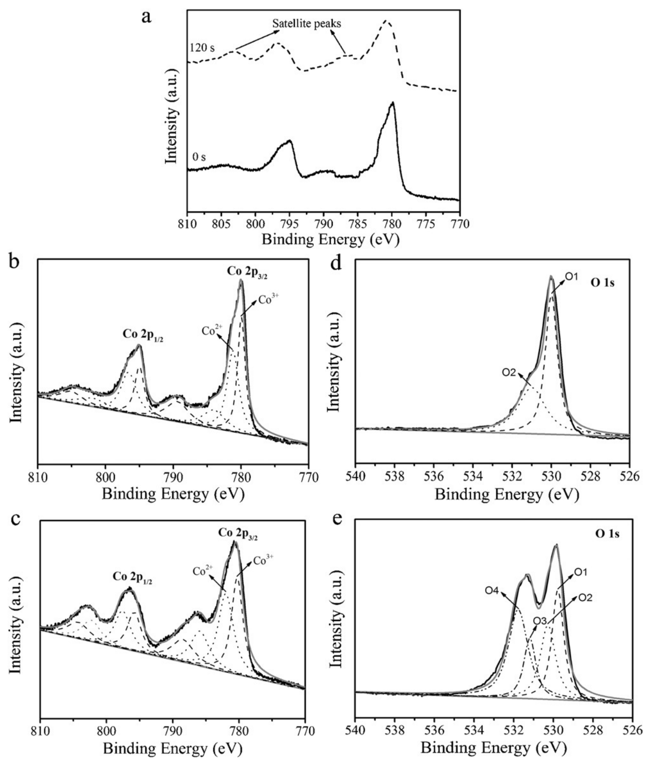

Figure 3. a) Co 2p XPS spectra of pristine Co_3O_4 and plasma engraved Co_3O_4. b), c) Fitted Co 2p for pristine Co_3O_4 (b) and for plasma-engraved Co_3O_4 (c). d), e) Fitted O 1s for pristine Co_3O_4 (d) and plasma-engraved Co_3O_4 (e).

To investigate the electrocatalytic performance for OER, the linear sweep voltammetry (LSV) curves of pristine Co_3O_4 nanosheets and plasma-engraved Co_3O_4 nanosheets are probed in alkaline electrolyte (0.1 M KOH), as shown in Figure 4 a. Since Co_3O_4 nanosheets were grown on Ti foil substrate, the supported electrocatalysts could be used as the working electrode directly. The onset potential for OER on Ar-plasma engraved Co_3O_4 nanosheets is 1.45 V versus RHE which is lower than pristine Co_3O_4 nanosheets (1.5 V vs. RHE). Furthermore, to reach the current density of 10 mA cm^{-2} (based on geometric electrode area), the pristine Co_3O_4 nanosheets requires a potential of 1.77 V versus RHE, while the plasma-engraved Co_3O_4 nanosheets only 1.53 V, suggesting the excellent electrocatalytic performance of Ar-plasma engraved Co_3O_4 nanosheets for OER. More apparently, the current density of OER on the plasma-engraved Co_3O_4 nanosheets is 44.44 mA cm^{-2} at 1.6 V, which is much higher than that of pristine Co_3O_4 nanosheets (2.57 mA cm^{-2}). The enhanced activity should be attributed to the unique surface properties of the plasma-engraved Co_3O_4 nanosheets with high surface area and oxygen vacancies. It is interesting to observe the specific activity (current per BET area) of the electrocatalyts for OER to understand the synergetic role of the surface area and oxygen vacancies. Thus, the current of the LSV curves in Figure 4 a were normalized by the BET surface area to exclude the contribution of the increased surface area to the significantly enhanced electrocatalytic activity of plasma-engraved Co_3O_4 for OER. The specific activity could exclusively specify the role of surface oxygen vacancies. Figure 4 b shows the LSV curves after normalizing

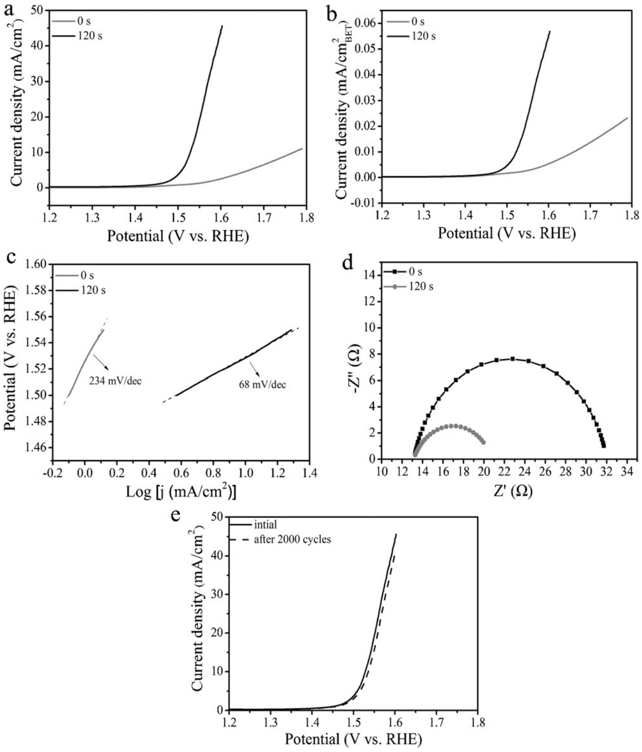

Figure 4. a) The polarization curves of OER on pristine Co_3O_4 (0 s) and the plasma engraved Co_3O_4 (120 s). b) The polarization curves normalized by the BET surface area. c) Tafel plots and d) Nyquist plots of OER on pristine Co_3O_4 and the plasma engraved Co_3O_4. e) Stability of the plasma-engraved Co_3O_4 after 2000 cycles.

the current in Figure 4a by the BET surface area. After the BET normalization, the specific activity of Ar-plasma engraved Co_3O_4 nanosheets is 0.055 mA cm^{-2}$_{BET}$ at 1.6 V, which is 10 times higher than that of pristine Co_3O_4 nanosheets (0.0054 mA cm^{-2}$_{BET}$), indicating the advanced catalytic activity of the Co_3O_4 surface after the plasma treatment contributed by the surface oxygen vacancies.

The Tafel slope is usually used to study the catalytic mechanism of electrocatalysis for OER.[17] In Figure 3c, the Tafel slope of Ar-plasma engraved Co_3O_4 is calculated to be 68 mV/dec, much lower than that of pristine Co_3O_4 (234 mV/dec). The Tafel slope comparison confirmed that the OER performance of Ar-plasma engraved Co_3O_4 is better than that of the pristine Co_3O_4. Furthermore, the turnover frequency (TOF) is also a very important kinetic parameter for OER. TOF is the intrinsic properties of the catalysts, which is important for evaluating the performance of the catalysts.[18] As summarized in the Supporting Information, Table S1, the TOF of Ar-plasma engraved Co_3O_4 is 0.21 s^{-1} at the overpotential of 0.3 V, while the TOF of the pristine Co_3O_4 was 0.02 s^{-1}. These electrochemical results indicated that the OER performance of Co_3O_4 was significantly improved by the plasma-engraving strategy with surface oxygen vacancies and high surface area. We tested the OER performance of treated Co_3O_4 for different plasma time (Supporting Information, Figure S8). It could be found that, initially, the activity increased with the increase of treatment time due to the increased surface area and the generation of oxygen vacancies. The best treatment time is found to be 120 s. The longer treatment results in poorer activity for OER because the over-treatment removed Co_3O_4 active species.

The electrochemical surface area (ECSA) is calculated by the cyclic voltammograms (CV) technique. In the Supporting Information, Figure S9, the double-layer capacitance (C_{dl}) of the Ar-plasma engraved Co_3O_4 nanosheets is about 94.97 mF cm^{-2}, which is much higher than pristine Co_3O_4 nanosheets (about 1.75 mF cm^{-2}). This result is consistent with the SEM, TEM, and BET characterizations. Moreover, the stability of electrocatalysts is very important for OER. As shown in the Figure 4e, Ar-plasma engraved Co_3O_4 nanosheets was tested by taking CV curves for 2000 cycles at a scan rate of 50 mV s^{-1}. There was only little decay of the activity based on the polarization curves after 2000 cycles. Furthermore, the electrochemical impedance spectroscopy (EIS) of Ar-plasma engraved Co_3O_4 nanosheets and the pristine Co_3O_4 nanosheets was tested at the onset potential (Figure 4d). The charge transfer resistance (R_{ct}) is closely related to the OER process. As can be seen in the Supporting Information, Figure S10, the R_{ct} of Ar-plasma engraved Co_3O_4 nanosheet is 7.7 Ω, which is much smaller than that of pristine Co_3O_4 nanosheet (18.8 Ω), indicating that Ar-plasma engraved Co_3O_4 nanosheets have relatively lower charge transfer resistance for OER.

As demonstrated in the Supporting Information, Figure S3, the plasma-engraving strategy could also be used to tailor NiO nanosheets. We also tested the electrochemical activity of NiO for OER. The LSV curves of pristine NiO and plasma engraved NiO for different time are shown in the Supporting Information, Figure S11a, and suggest that the OER performance of plasma engraved NiO is better than pristine NiO. The Tafel slope of Ar-plasma engraved NiO is lower than pristine NiO (Figure S11b). The EIS test of Ar-plasma engraved NiO and the pristine NiO indicates that the Ar-plasma engraved NiO shows lower charge transfer resistance (7 Ω) than pristine NiO (11.1 Ω; Figure S11c, Figure S12). Like Co_3O_4, the plasma-treated NiO nanosheets also show reasonable stability (Figure S11d). The electrochemical surface area of Ar-plasma engraved NiO nanosheet is also higher than the pristine NiO nanosheets (Supporting Information, Figure S13). All of these electrochemical results conclude similarly like the Co_3O_4-related studies above.

Previous studies on the facet-dependence of the Co_3O_4 for electrocatalysis have demonstrated that the population of Co^{2+} and Co^{3+} on different exposed facets of Co_3O_4 nanostructures is the key to influence the catalytic performance. The relative population of Co^{2+} over Co^{3+} is directly related to the oxygen vacancies. The high OER catalytic activity of Co_3O_4 has been attributed to high Co^{2+} population. Liu et al. performed the in-operando identification of geometrical-site-dependent OER activity of spinel Co_3O_4 and concluded that Co^{2+} was the active sites for OER and Co^{2+} could promote the formation of cobalt oxyhydroxide (CoOOH) as active sites for OER.[19] Therefore, increasing the population of Co^{2+} (oxygen vacancies) in Co_3O_4 could significantly enhance the electrocatalytic activity for OER. Herein, the as-developed plasma-engraving strategy not only increased the surface area of Co_3O_4 nanosheets, but also led to the formation of oxygen vacancies on the surface of Co_3O_4 nanosheets. The synergistic effect of the surface oxygen vacancies and high surface area of Co_3O_4 nanosheets result in a superior electrocatalyst for OER.

In summary, we have demonstrated a simple but efficient plasma-engraving strategy to produce Co_3O_4 nanosheets with oxygen vacancies and high surface area. The electrocatalytic performance of Co_3O_4 for OER is mainly affected by its surface area and the oxygen vacancies, both of which could be simultaneously realized by the plasma-engraving method. In addition to the usual contribution of the high surface area, the specific activity results (mA per BET area) imply the significant role of the oxygen vacancies. The plasma-engraving method is green, efficient and safe. The electrocatalytic activity for OER of metal oxides could be significantly enhanced through proper surface engraving by plasma. With the plasma engraving, although less electrocatalyst resided, more active sites, and better catalytic activity were realized by obtaining the high surface area and oxygen vacancies. Therefore, the as-developed plasma-engraving strategy could produce highly competitive non-noble electrocatalysts for oxygen production from water splitting. This work provides a new strategy to design advanced electrocatalysts by increasing the surface area and generating surface oxygen vacancies simultaneously.

Acknowledgements

The authors acknowledge the support from the National Natural Science Foundation of China (51402100 and 21573066).

Keywords: Co_3O_4 · electrocatalysis · oxygen evolution · oxygen vacancies

How to cite: *Angew. Chem. Int. Ed.* **2016**, *55*, 5277–5281
Angew. Chem. **2016**, *128*, 5363–5367

[1] N. S. Lewis, D. G. Nocera, *Proc. Natl. Acad. Sci. USA* **2006**, *103*, 15729–15735.
[2] J. Z. Zhu, X. D. Ren, J. J. Liu, W. Q. Zhang, Z. Y. Wen, *ACS Catal.* **2015**, *5*, 73–81.
[3] Y. Liang, Y. Li, H. Wang, J. Zhou, J. Wang, T. Regier, H. Dai, *Nat. Mater.* **2011**, *10*, 780–786.
[4] T. Y. Ma, S. Dai, M. Jaroniec, S. Z. Qiao, *J. Am. Chem. Soc.* **2014**, *136*, 13925–13931.
[5] X. X. Zou, J. Su, R. Silva, A. Goswami, B. R. Sathe, T. Asefa, *Chem. Commun.* **2013**, *49*, 7522–7524.
[6] Z. Chen, C. X. Kronawitter, B. E. Koel, *Phys. Chem. Chem. Phys.* **2015**, *17*, 29387–29393.
[7] Y. C. Wang, T. Zhou, K. Jiang, P. M. Da, Z. Peng, J. Tang, B. A. Kong, W. B. Cai, Z. Q. Yang, G. F. Zheng, *Adv. Energy Mater.* **2014**, *4*, 1400696.
[8] R. Gao, Z. Li, X. Zhang, J. Zhang, Z. Hu, X. Liu, *ACS Catal.* **2016**, *6*, 400–406.
[9] a) Z. Li, Q. Q. Jiang, Z. L. Ma, Q. H. Liu, Z. J. Wu, S. Y. Wang, *RSC Adv.* **2015**, *5*, 79473–79478; b) L. Tao, X. D. Duan, C. Wang, X. F. Duan, S. Y. Wang, *Chem. Commun.* **2015**, *51*, 7470–7473; c) Q. Q. Jiang, Z. Li, S. Y. Wang, H. Zhang, *RSC Adv.* **2015**, *5*, 92995–93001; d) S. Dou, L. Tao, J. Huo, S. Wang, L. Dai, *Energy Environ. Sci.* **2016**, DOI: 10.1039/C6EE00054A.
[10] A. K. Engstfeld, S. Brimaud, R. J. Behm, *Angew. Chem. Int. Ed.* **2014**, *53*, 12936–12940; *Angew. Chem.* **2014**, *126*, 13150–13154.
[11] R. G. Haverkamp, A. T. Marshall, B. C. C. Cowie, *Surf. Interface Anal.* **2011**, *43*, 847–855.
[12] a) S. C. Petitto, E. M. Marsh, G. A. Carson, M. A. Langell, *J. Mol. Catal. A* **2008**, *281*, 49–58; b) J. Zhu, K. Kailasam, A. Fischer, A. Thomas, *ACS Catal.* **2011**, *1*, 342–347.
[13] H. Wang, C. Qing, J. Guo, A. A. Aref, D. Sun, B. Wang, Y. Tang, *J. Mater. Chem. A* **2014**, *2*, 11776–11783.
[14] a) H. Tüysüz, Y. Liu, C. Weidenthaler, F. Schüth, *J. Am. Chem. Soc.* **2008**, *130*, 14108–14110; b) L. Liao, Q. Zhang, Z. Su, Z. Zhao, Y. Wang, Y. Li, X. Lu, D. Wei, G. Feng, Q. Yu, X. Cai, J. Zhao, Z. Ren, H. Fang, F. Robles-Hernandez, S. Baldelli, J. Bao, *Nat. Nanotechnol.* **2014**, *9*, 69–73.
[15] Y. Chen, H. Wang, C.-J. Liu, Z. Zeng, H. Zhang, C. Zhou, X. Jia, Y. Yang, *J. Catal.* **2012**, *289*, 105–117.
[16] K. Navaneetha Pandiyaraj, R. R. Deshmukh, A. Arunkumar, M. C. Ramkumar, I. Ruzybayev, S. I. Shah, P. G. Su, M. H. Periayah, A. S. Halim, *Appl. Surf. Sci.* **2015**, *347*, 336–346.
[17] F. Song, X. Hu, *J. Am. Chem. Soc.* **2014**, *136*, 16481–16484.
[18] A. J. Esswein, M. J. McMurdo, P. N. Ross, A. T. Bell, T. D. Tilley, *J. Phys. Chem. C* **2009**, *113*, 15068–15072.
[19] H.-Y. Wang, S.-F. Hung, H.-Y. Chen, T.-S. Chan, H. M. Chen, B. Liu, *J. Am. Chem. Soc.* **2016**, *138*, 36–39.

Received: January 21, 2016
Published online: March 17, 2016

